Nishizawa *et al. Earth, Planets and Space* (2017) 69:86
DOI 10.1186/s40623-017-0674-7

Earth, Planets and Space

FULL PAPER Open Access

Variations in seismic velocity distribution along the Ryukyu (Nansei-Shoto) Trench subduction zone at the northwestern end of the Philippine Sea plate

Azusa Nishizawa*, Kentaro Kaneda, Mitsuhiro Oikawa, Daishi Horiuchi, Yukari Fujioka and Chiaki Okada

Abstract

The Ryukyu (Nansei-Shoto) island arc-trench system, southwest of Japan, is formed by the subduction of the Philippine Sea (PHS) plate. Among the subduction zones surrounding the Japan Islands, the Ryukyu arc-trench system is unique in that its backarc basin, the Okinawa Trough, is the area with current extensively active rifting. The length of the trench is around 1400 km, and the geological and geophysical characteristics vary significantly along the trench axis. We conducted multichannel seismic (MCS) reflection and wide-angle seismic surveys to elucidate the along-arc variation in seismic structures from the island arc to the trench regions, shooting seven seismic lines across the arc-trench system and two along-arc lines in the island arc and the forearc areas. The obtained *P*-wave velocity models of the Ryukyu arc crust were found to be heterogeneous (depending on the seismic lines), but they basically consist of upper, middle, and lower crusts, indicating a typical island arc structure. Beneath the bathymetric depressions cutting the island arc—for example, the Kerama Gap and the Miyako Saddle—the MCS record shows many across-arc normal faults, which indicates the presence of an extensional regime along the island arc. In the areas from the forearc to the trench, the subduction of the characteristic seafloor features on the PHS plate affects seismic structures; the subducted bathymetric high of the Amami Plateau is detected in the northern trench: the Luzon–Okinawa fracture zone beneath the middle and southern trenches. There are low-velocity (<~4.5 km/s) wedges along the forearc areas, except for off Miyako-jima Island. The characteristic high gravity anomaly at the forearc off Miyako-jima Island is caused not by a bathymetric high of a large-scale accretionary wedge but by shallower materials with a high *P*-wave velocity of ~4.5 km/s.

Introduction

The Ryukyu (Nansei-Shoto) island arc exists at the southwest of the Japan island arc and forms a typical arc-trench system. The Philippine Sea (PHS) plate is subducting along the Ryukyu Trench at a rate of around 98 mm/year northwestward (Sella et al. 2002). Since the strike of the trench axis varies at around 126°E, the plate subduction is perpendicular to the axis in the north and oblique in the south. The Ryukyu arc-trench system is unique in the subduction zones around Japan in terms of the existence of an active backarc basin, the Okinawa Trough (Fig. 1).

The Ryukyu arc-trench system is generally divided into three parts based on topography, geology, biology, and other characteristics. The most significant topographic boundaries are two large bathymetric depressions: the Tokara Valley between the Tokara Islands and the Amami Islands in the northern arc, and the Kerama Gap between Okinawa Island and Miyako-jima Island in the southern arc. Both depressions are offset by large-scale left-lateral strike–slip faults (Matsumoto et al. 1996). Other than the two major gaps, there are several large topographic saddles across the southern island arc. In the backarc basin (the Okinawa Trough), the water depth generally

*Correspondence: azusa@mail1.accsnet.ne.jp
Hydrographic and Oceanographic Department, Japan Coast Guard, Tokyo 100-8932, Japan

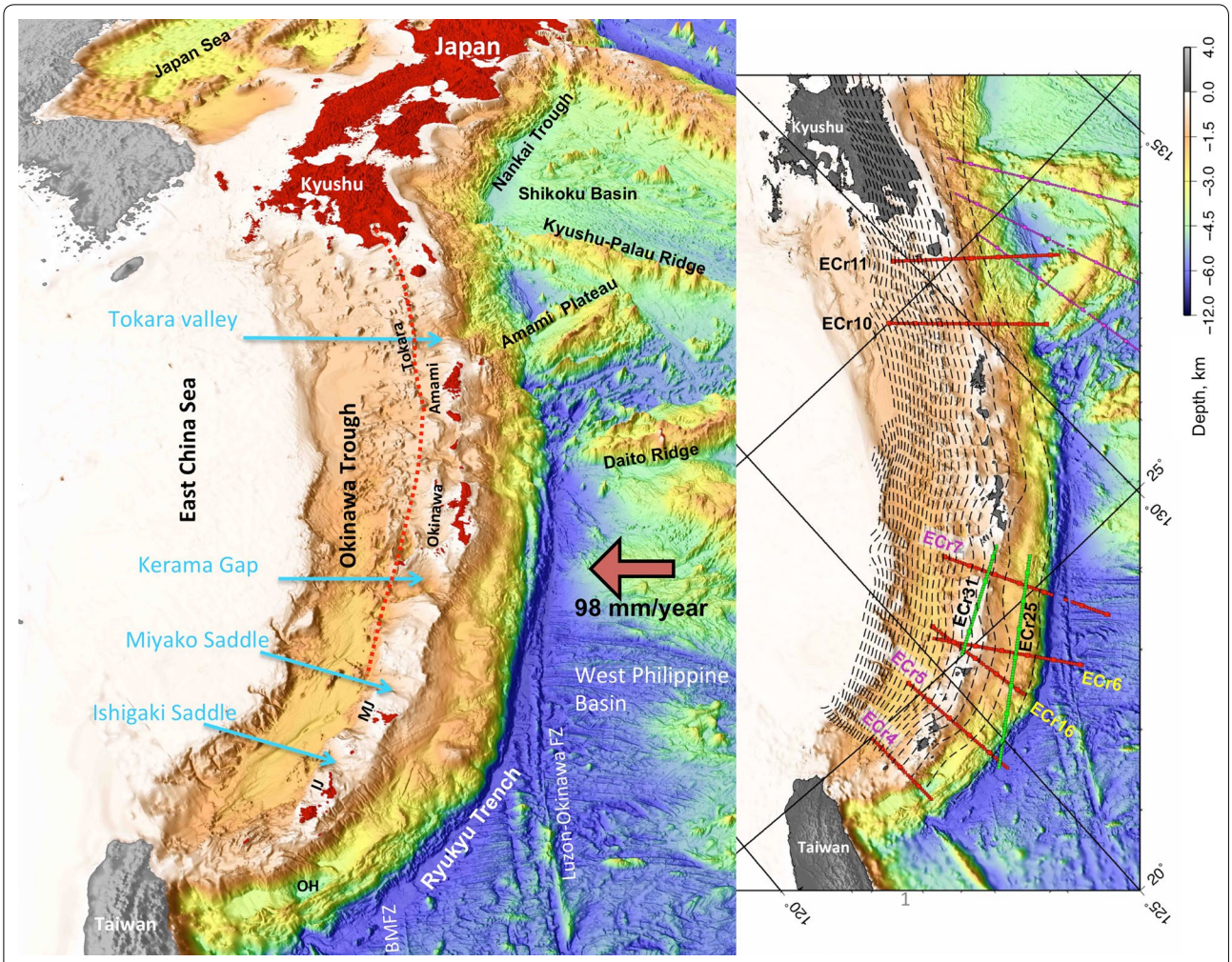

Fig. 1 Tectonic maps and locations of seismic lines. The characteristic seafloor topography of the Philippine Sea plate on the *left* and the position of the seismic lines (*red* and *green lines*) across and along the Ryukyu (Nansei-Shoto) arc on the *right*. The rough position of the volcanic front is shown in *red dotted line*. *Three thin violet lines* are previous seismic lines across the northernmost Ryukyu Trench (Nishizawa et al. 2009). A non-tuned airgun array with a capacity of 6000 (1500 × 4) cubic inch (98.3 L) was shot for the refraction survey and a 1050 (350 × 3) cubic inch (17.2 L) airgun cluster was used for the multichannel reflection survey. *Broken lines* indicate iso-depth contours of the plate interface with an interval of 10 km (Hayes et al. 2012). *MJ* Miyako-jima, *IJ* Ishigaki-jima, *BMFZ* Botan-Miyako fracture zone, *OH* Oki-Hateruma Basin

increases from north to south and the seafloor topography in the trough also shows a north–south variation as a boundary at the northwestward extension of the Kerama Gap. Several conspicuous en echelon graben structures are characterized along the center of the southern trough, while similar features are unclear in the northern trough. At the transition from arc to trough, a volcanic front is recognizable in the northern region; however, one is not clear in the south. Along-arc variations in seafloor features prevail in the whole of the Ryukyu arc-trench-back-arc system.

The seafloor topography of the subducting PHS plate also varies along the trench axis. In the northern parts, there are several bathymetric highs such as the Amami Plateau and the Daito Ridge on the PHS plate subducting below the trench. Meanwhile, the Luzon–Okinawa fracture zone (LOFZ) in the middle and southern regions and the Gagua Ridge in the southwest subduct beneath the trench and deform the forearc seafloor.

Figure 2 shows three geophysical maps illustrating free-air gravity anomaly, seismic activity, and magnetic anomaly. The free-air gravity anomaly generally reflects the seafloor topography and shows lower gravity anomalies at the major bathymetric depressions cut the along-arc high gravity anomaly (Fig. 2a). Another characteristic in the gravity map is that there are two low gravity anomaly belts parallel to the trench. One of the low gravity belts is along the trench axis, and the other one is in the

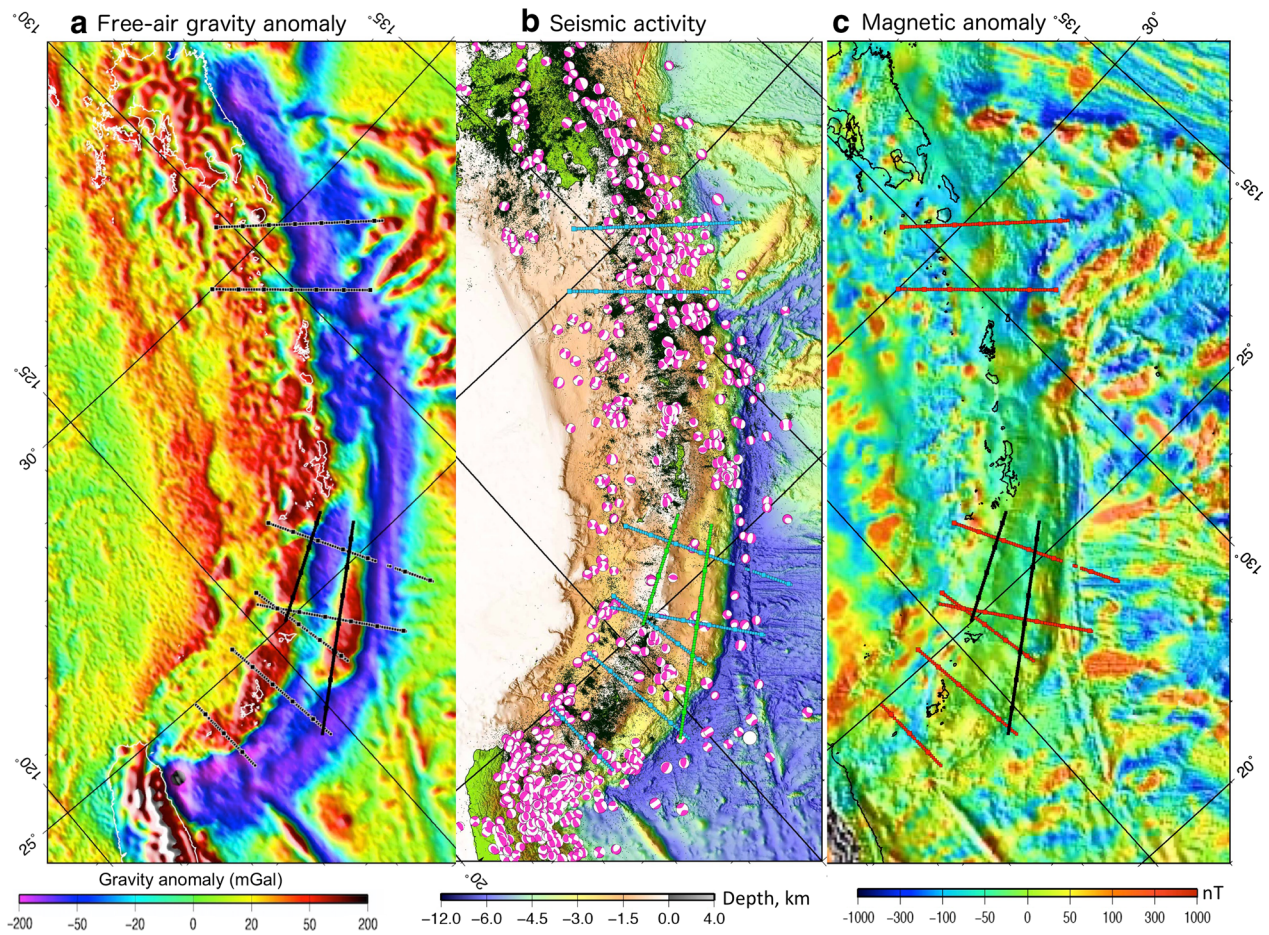

Fig. 2 Geophysical maps of the survey area. **a** Free-air gravity anomaly. **b** Shallow seismic activity. *Black dots* show epicenters with depths shallower than 60 km as determined by the Japan Metrological Agency (1923–2017 Feb. 20). Focal mechanisms are from GCMT Catalog by Global Centroid-Moment-Tensor Project (depth ≤ 60 km, 1976–2017 May 31). **c** Magnetic anomaly on bathymetry. The magnetic anomaly map is produced by a combination of our original data, CCOP (http://www.ccop.or.th/), and EMAG2 (doi:10.7289/V5MW2F2P)

forearc region, especially between off Miyako-jima Island and Okinawa Island. Similar features are observed along the forearc of the Nankai Trough, the seismogenic zone of large earthquakes (e.g., Wells et al. 2003). Figure 2b shows shallow seismicity at depth ≤60 km in the Ryukyu region. The distribution of subduction-related earthquakes varies along the arc, and the seismicity is slightly low in the forearc high gravity anomaly area between off Miyako-jima Island and off Okinawa Island. The most distinctive feature of the magnetic anomaly (Fig. 2c) is that many dipolar anomalies related to the bathymetric highs on the PHS plate—such as the Kyushu-Palau Ridge, the Amami Plateau, and the Daito Ridge—are subducting beneath the trench. The anomalies can be traced to the forearc area.

Several seismic explorations have been conducted in the Ryukyu region, and they have yielded *P*-wave velocity (*Vp*) models of PHS plate subduction-related structures and backarc rifting-related structures (e.g., Hirata et al. 1991; Iwasaki et al. 1990; Kodaira et al. 1996; Nakahigashi et al. 2004; Klingelhoefer et al. 2012). However, the number of seismic surveys conducted in this area is very small compared to those made in the Nankai Trough and the Japan Trench, which are seismogenic plate subduction zones around Japan. This is because the interplate coupling in the Ryukyu subduction zone is considered to be weak, based on the fact that there are few records of large earthquakes in the region, although the 1771 Meiwa Tsunami (Yaeyama Earthquake: *M*~8) and 1911 Kikai-jima Earthquake (*M*8) both occurred around the Ryukyu Trench. However, Goto (2013) proposed that the great Kikai-jima Earthquake is the interplate event and Ando et al. (2012) suggested that there are coupled regions within the accretionary prism or at the plate interface,

based on the locations and the mechanisms of very low frequency earthquakes. Moreover, the double low gravity belts in the forearc region may reflect strong interplate coupling as suggested by Song and Simons (2003) and Tan et al. (2012). After the disastrous 2004 Sumatra-Andaman earthquake (Mw 9.3), several studies (e.g., Hsu and Sibuet 2005; Lin et al. 2014) pointed out that the tectonic backgrounds between the source area of the Sumatra-Andaman earthquake and the Ryukyu Trench are very similar. Besides, the 2011 Tohoku-oki earthquake (Mw 9.0) taught us the importance of there being very few geological records of giant earthquakes with a very long recurrence interval. Therefore, the seismic structure related to the PHS plate subduction is very important in estimating the potential for massive devastating earthquakes in the Ryukyu Trench region.

Recently, several extensive seismic surveys have been conducted to investigate the relationship between seismic structure and seismic activity in the Ryukyu Trench subduction zone. For instance, Hsu et al. (2013) discussed the mega-splay fault system detected by an MCS survey and tsunamigenic faults such as the 1771 Meiwa Tsunami, while Arai et al. (2016) investigated the fault structure and seismic activity on the basis of passive and active observations in the southern Ryukyu Trench. However, it is difficult to conduct such extensive seismic surveys over the entire Ryukyu Trench region since the trench is very long, about 1400 km, and is far from Honshu, the main island of Japan. The Japan Coast Guard has been collecting basic geological and geophysical data in and around the Ryukyu island arc area since 2008. Here, we will summarize the results obtained to date from seven seismic refraction lines across the Ryukyu Trench and two lines along the arc and forearc, and characterize variations of the V_p structure from the trench to the transition to the Okinawa Trough. Okamura et al. (2017) discuss the subsidence of the forearc wedge of the Ryukyu Arc based on the results of this paper. We will report V_p models for the Okinawa Trough in a future paper.

Data acquisition and analyses

We conducted nine lines of seismic refraction/reflection survey in the Ryukyu Trench subduction zone (Fig. 1): Seven of them cross the Ryukyu island arc, two in the north and five in the south, and the remaining two lines were shot along the island arc and the forearc area in the southern Ryukyu arc.

In the reflection surveys, we used a 3000-m-long, 240-channel hydrophone streamer as a receiver for the across-trench lines, and a 3000-m-long, 480-channel streamer was operated for the ECr25 and ECr31 along-trench lines. An airgun cluster with a total volume of 17.1 L (1050 cubic inches) was shot at 50-m intervals as a controlled seismic source. We processed the MCS data using standard techniques and obtained a depth-converted profile for each line. In the refraction survey, we deployed ocean bottom seismographs (OBS) at 5-km intervals and shot a non-tuned airgun array with a total volume of 98.4 L (6000 cubic inches) at 200-m intervals (around 90 s). Navigation was provided by the ship's global positioning system, and each OBS instrument was relocated using direct water wave arrivals (Oshida et al. 2008).

Each OBS was equipped with a three-component 4.5-Hz geophone and a hydrophone, and we mainly used vertical and hydrophone outputs. Since the maximum water depth limit for the hydrophone sensor is 6000 m, we deployed the OBSs without hydrophones at positions deeper than 6000 m. The procedures for the OBS data analysis are the same as those summarized by Nishizawa et al. (2014). Constructing V_p models, we used information about the shallow sedimentary structures and depths of the subducting PHS plate interface deduced from MCS survey. As there were ample ray paths in V_p models shallower then 10 km, we obtained upper crust V_p models by means of a tomo2d tomographic inversion (Korenaga et al. 2000) for the observed travel times of first arrivals. Misfits of the tomographic inversion were less than 50 ms for nearly all V_p models. We examined the resolution of the results using conventional checkerboard tests and ray coverage. However, we estimated deeper structures at depths greater than 10 km by forward modeling with two-dimensional ray tracing (Fujie et al. 2000; Kubota et al. 2009) using intermittent reflection signals and weak and distant refraction signals. The forward modeling based on several critical reflection signals was very effective in identifying velocity discontinuities in the crust. Furthermore, we confirmed the V_p models by comparing observed record sections with synthetic seismograms calculated by a finite difference method, E3D (Larsen and Schultz 1995).

Results

Depth-converted MCS profiles and V_p models for seven seismic lines perpendicular to the trench axis are shown in Figs. 3 and 4, respectively, while the checkerboard test result and the ray diagram for each line are shown in Fig. 5. Ray diagrams for ECr6 and ECr4 in Fig. 5 show ray paths from several reflectors in the upper mantle of the island arc and the PHS plate. These reflectors were inferred to explain the travel times of later phases with large amplitude observed at several OBSs. However, since the positions of the reflectors were not so accurate due to uncertain mantle velocities, we did not show them in the V_p models in Fig. 4. Below we describe the characteristics of the models from north to south, and from the island arc to the trench area.

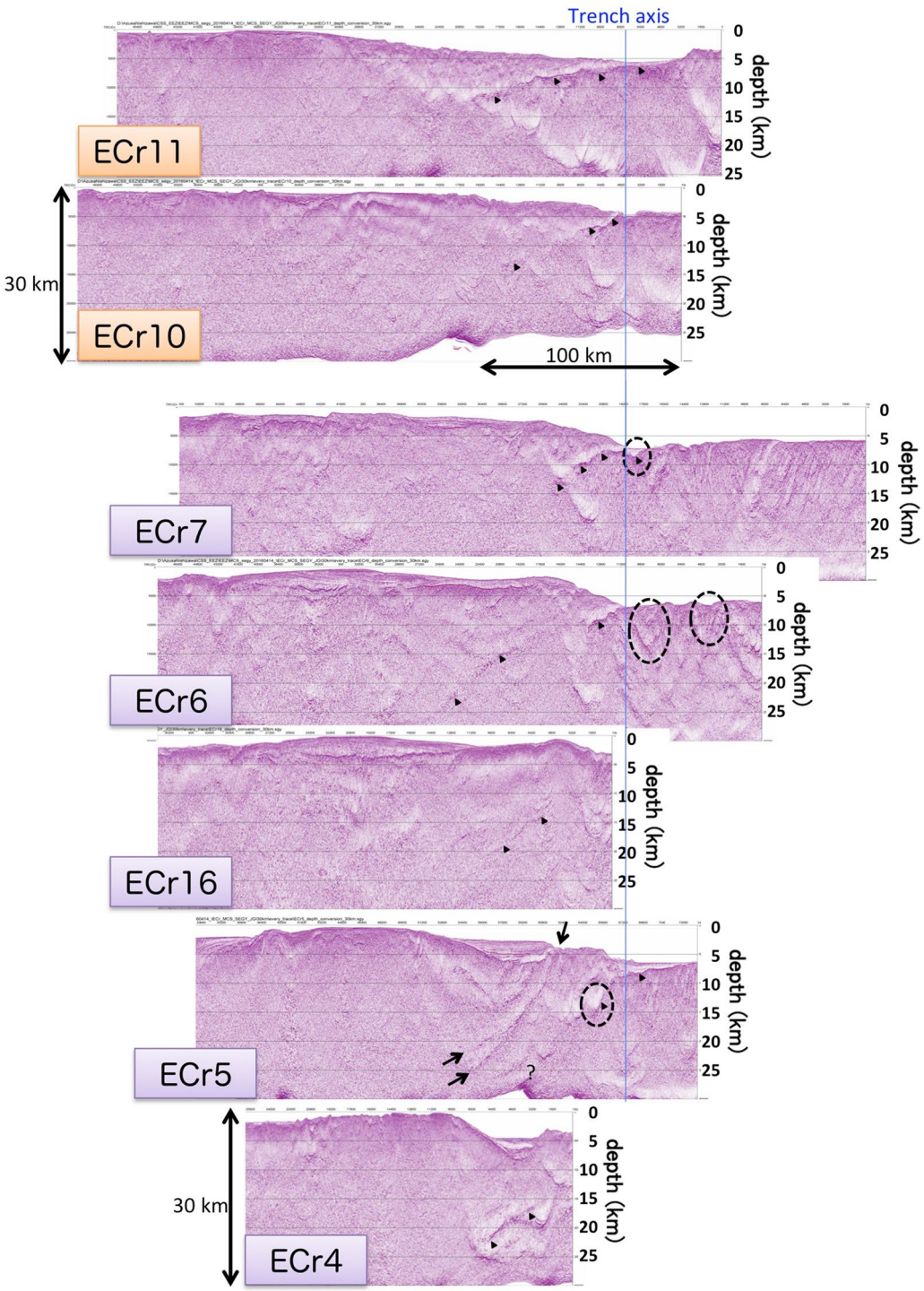

Fig. 3 Multichannel seismic profiles (depth-converted section) for the across-trench survey lines. The *vertical blue line* shows the positions of the trench axis. The *triangles* and *dashed ellipses* indicate the estimated positions of the subducting Philippine Sea plate interface and the fracture zone, respectively. The *arrows* in ECr5 indicate a possible splay fault

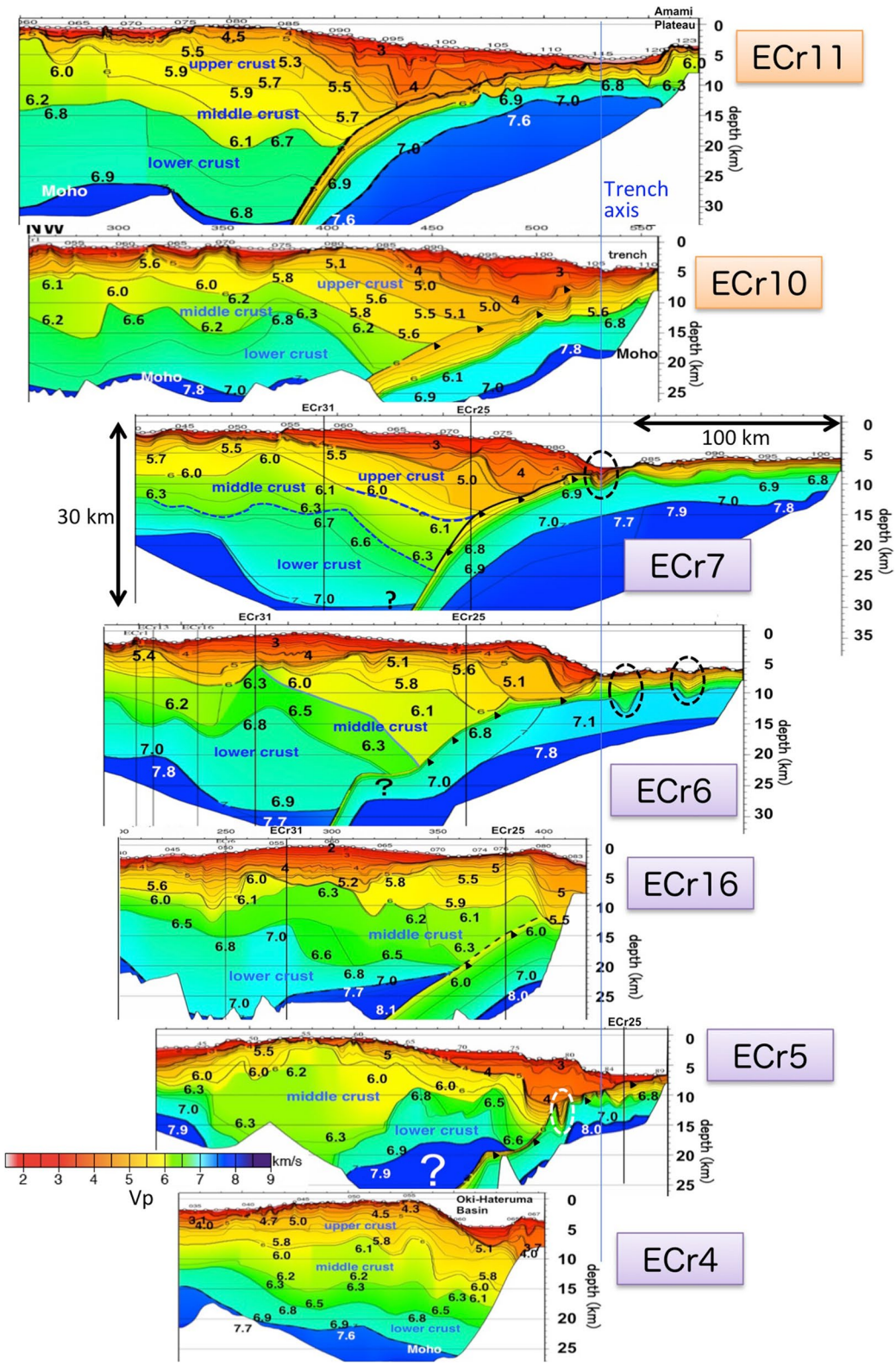

Fig. 4 *P*-wave velocity models for the survey lines perpendicular to the trench axis. The *contour* interval is 2.5 km/s. The *vertical blue line* shows the position of the trench axis. The *triangles* and *dashed ellipses* indicate the estimated positions of the subducting PHS plate interface and the fracture zone, respectively

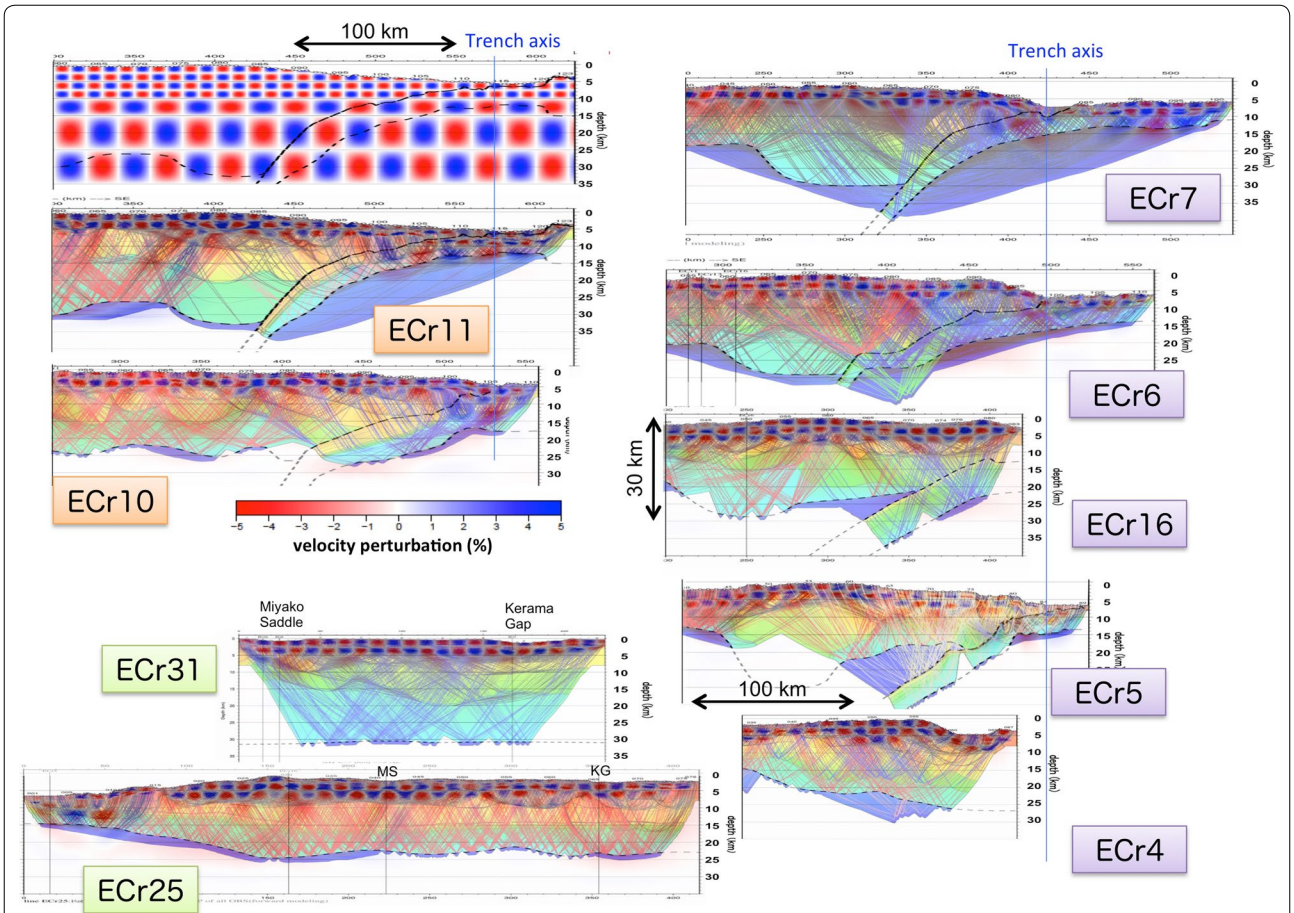

Fig. 5 Resolution of each *P*-wave velocity model. The *top left* shows the checkerboard test initial pattern of the tomographic inversion for ECr11. Ray coverage is also plotted from the forward modeling, including reflection waves

Northern Ryukyu (ECr11 and ECr10)

ECr11 and ECr10 were shot across the northern Ryukyu arc-trench system. Both seismic lines intersect with the volcanic front associated with the PHS plate subduction below the Ryukyu arc. ECr10 is positioned along the Tokara Valley area, a left-lateral strike–slip fault and the boundary between the north and the middle Ryukyu arc (e.g., Matsumoto et al. 1996). We show some examples of the OBS record sections and forward modeling results for ECr11 in Fig. 6. Although the characteristics of each record section differ depending on its position on the seismic line, many reflection signals from inside the arc crust and base of the crust (Moho) were identified among the record sections. We carefully picked the first arrivals, the reflection signals from the upper/middle crust boundary, middle/lower crust boundary, the Moho discontinuity, and other distinctive signals. Then we conducted the tomographic inversion and forward modeling using these travel-time data. In particular, we tried to construct V_p models with a layered structure by means of forward modeling in consideration of the appearance of the reflection signals. V_p models and ray diagrams for ECr11 and ECr10 are shown in Figs. 4 and 5, respectively.

We divided the arc crust into three parts, mainly on the basis of the *P*-wave velocity for each crustal part and the velocity gaps among the parts. Figure 6 shows examples of reflection signals from several velocity discontinuities for ECr11. The arc crust below ECr11 consists of thin uppermost sediments: an upper crust with a V_p of 4–5.7 km/s, a middle crust with a V_p of 5.9–6.1 km/s, and a lower crust with a V_p of 6.7–6.8 km/s. The V_p model for the arc beneath ECr10 has an upper crust with a V_p that is less than 5.8 km/s, a middle crust with a V_p of 6.0–6.3 km/s, and a lower crust with a V_p 6.6–7.0 km/s. There are no positive evidences for the existence of the Moho transition layer. However, we should consider that the refracted waves propagating through the arc lower crust are concentrated at the top of the layer, as shown in the ray diagram in Fig. 5, due to its rather constant velocity. In addition, because of few PmP signals from the arc

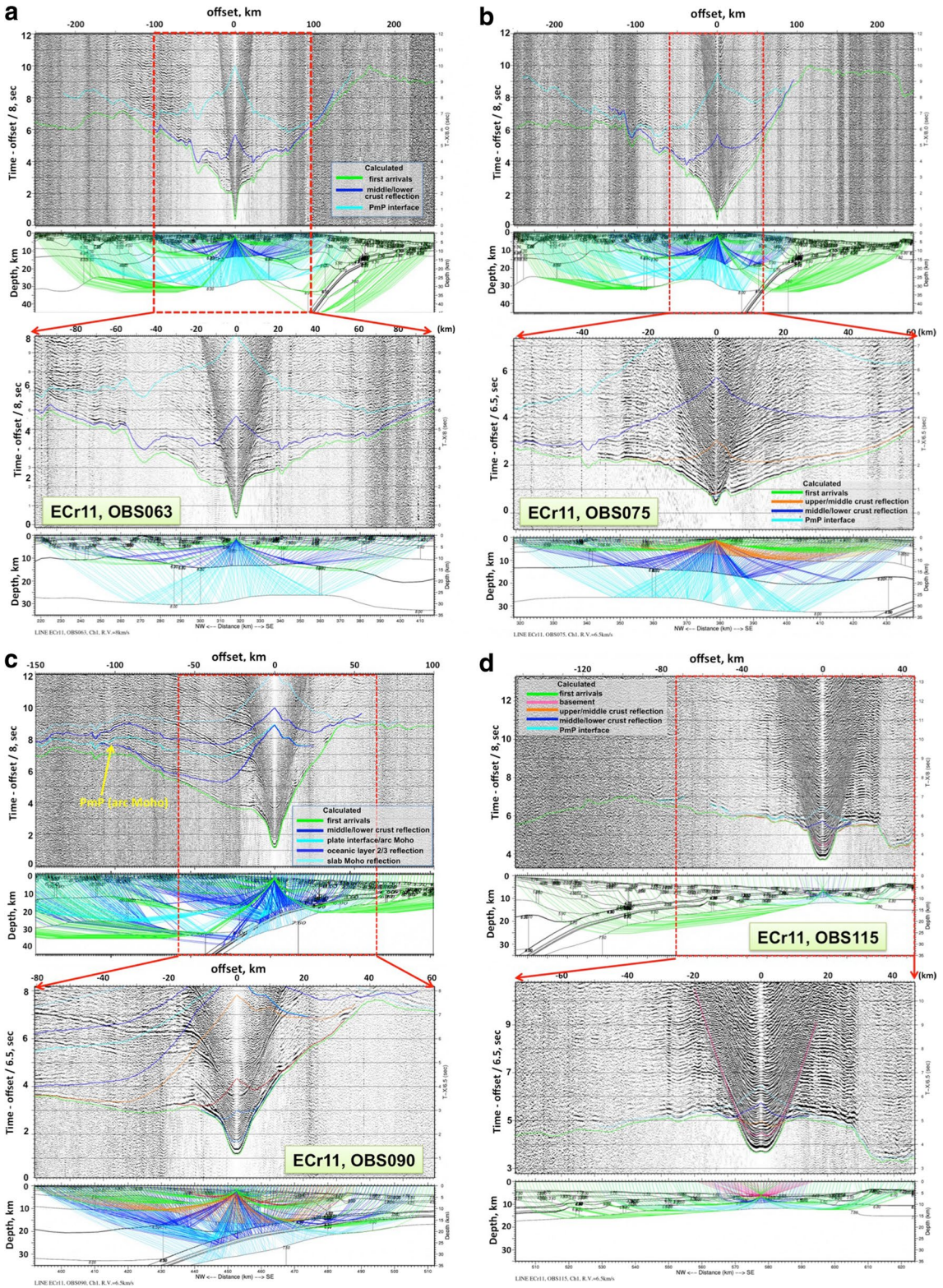

Fig. 6 Example of forward modeling for ECr11. **a** OBS063, **b** OBS075, **c** OBS090, **d** OBS115. Vertical record sections with calculated travel times and ray diagram are shown for each OBS. The OBS data were processed through predictive deconvolution and band-pass filtered (4–20 Hz). A gain factor proportional to distance has been used to enhance the distant seismograms. The color of the calculated travel times corresponds to the ray path in the ray diagram

Moho, we could not constrain the velocity at the bottom of the crust using the PmP amplitude data.

The Moho depth of the Ryukyu island arc for ECr11 is estimated to be around 33 km, based on the PmP signals recorded by OBS090, as shown in Fig. 6c. The depth, however, may be slightly shallower if ~0.2 s smaller travel times that match the very weak signals recorded by some of the other OBSs are taken into consideration. We could not determine the depth of the arc Moho below ECr10 because clear Moho reflections were not observed. For ECr11, we tried to determine the V_p of the uppermost mantle beneath the arc by using Moho reflections of the subducting PHS plate (e.g., Fig. 6c), but the fitting between the observed and the calculated travel times sometimes shows errors of around 0.5 s. Therefore, the mantle wedge structure could not be well resolved either.

In the forearc area, a sedimentary wedge with $V_p \leq 5$ km/s and a maximum thickness of 10 km exist along ECr11 and ECr10. Only a few weak signals from the middle and lower arc crusts below ECr10 were observed, which was apparently due to the attenuation of seismic energy in the Tokara Valley area.

Clear reflections from the top of the subducting PHS plate, with a slightly irregular topography related to the Amami Plateau in the MCS records, were detected down to a depth of 13 km for ECr11 (Fig. 3). However, reflection events from the plate interface deeper than 8 km could barely be traced for the MCS record for ECr10, perhaps due to the larger seafloor irregularities caused by the Amami Plateau.

Southern Ryukyu (ECr7, ECr6, ECr16, ECr5, and ECr4)

Five lines, ECr7, ECr6, ECr16, ECr5, and ECr4, from north to south, were located approximately perpendicular to the strike of the southern Ryukyu Trench. ECr7, ECr6, and ECr5 cross into the trench axis, but ECr16 and ECr4 do not extend to the axis. All the lines traversed the slightly depressed areas of the island arc so that the survey vessel could continue to shot the airgun along the lines.

ECr7 was designed along the bathymetric depression (the Kerama Gap) in the island arc and forearc area. Materials with $V_p < 5$ km/s are present at the top of the whole island arc and forearc area, with a maximum thickness of 9 km beneath the forearc (Fig. 4). We interpreted the layers with a $V_p \leq 6.0$ km/s and a $V_p = 6.0$–6.3 km/s as the upper curst and a middle crust, respectively. Since we could not determine the Moho depth below the arc crust in ECr7, we placed the Moho depth at 30 km based on the results from ECr6 and ECr31. On the basis of this setting, we tried to adjust the V_p model to explain distant signals with offsets greater than ~80 km that propagated through the mantle wedge. Below the trench, we could obtain clear images of the subducting LOFZ with bumped topographies from both the MCS profile (Fig. 3) and the V_p model (Fig. 4). The reflection signals from the top of the plate boundary could be traced to around 10 km from the sea bottom in the MCS records (Fig. 3).

ECr6 is located along the Miyako Saddle, a slightly smaller seafloor depression than the Kerama Gap. Materials with $V_p < 5$ km/s prevail from the island arc to the forearc area; however, the distribution of the low-V_p materials at the front of the forearc is narrower than those of ECr11, ECr10, and ECr7. Since it is difficult to determine the boundary between the upper crust and lower crust, we interpreted the areas with a V_p of 6.1–6.5 km/s as the middle crust below the island arc and forearc based on their velocities. The arc Moho depth of about 29 km is estimated from PmP arrivals (see the checkerboard test result in Fig. 5). The V_p model beneath the forearc differs significantly from that of ECr7, where materials with a fast V_p of around 5 km/s exist at shallow depths within 2–3 km from the seafloor. In the trench region, the LOFZ, a rough topography with a width of about 50 km, is subducting at the eastern end of ECr6 (Fig. 1). The MCS record of ECr6 shows a blurred image of the LOFZ below the seafloor (Fig. 3). In contrast, we could obtain clear reflection signals from the subducting plate interface down to a depth greater than 20 km in the MCS record.

ECr16 also passes along the Miyako Saddle and crosses ECr6 in the island arc area. Since ECr16 is near ECr6, their crustal models are similar to the depth of the upper crustal layer. A middle crust with a V_p of 6.1–6.6 km/s is estimated beneath the island arc and forearc area. The depth of the arc Moho was inferred from reflection signals. Refection signals from the subducting PHS plate were observed in the MCS record, while they were not as clear as those for ECr6 (Fig. 3).

ECr5 passes through a seafloor depression of the Ishigaki Saddle, which is rather smaller compared to the Kerama Gap and the Miyako Saddle. The V_p structure below the island arc is very different from that of ECr6 and ECr16. There is no thick, low-velocity sediment in the shallow island arc area, and materials with a V_p of around 5 km/s ascend to a shallower depth. Thick upper and middle crusts characterize the arc crust in this line. A middle crust with a V_p of 6.0–6.3 km/s is widely distributed to a depth of 20 km from the sea surface. The thickness of the lower crust and the Moho depth were not well determined, because there were very few reflection signals from the Moho, indicating no distinctive Moho discontinuity.

In spite of the flat seafloor in the trench axis area along ECr5, a large undulation of the subducting plate interface, shown in the ellipse in Fig. 3, can be identified below

the landward slope of the trench. This irregularity is also detected in the V_p model, where the low-V_p upper oceanic crust extends to the lower crust (Fig. 4). This might be related to a northern extension of the Botan-Miyako fracture zone, a slightly smaller fracture zone almost parallel to the LOFZ (Fig. 1). The MCS records show there are several reflection signals with large amplitudes beneath the forearc basin (Fig. 3). Although the southernmost reflector appears to be the subducting plate interface shown by triangles, the reflector, having depth >10 km, is irregular and broken.

Estimation of the mantle wedge structure was very difficult. Although we examined several models using forward modeling, we could not find an optimal model. In the V_p model shown in Fig. 4, we interpreted the large amplitude signals that occurred with a velocity discontinuity at a depth of ~18 km as being island arc Moho reflections. However, these signals might be reflections from the inner lower crust or from the top of the subducting PHS plate. Further examinations are necessary to constrain the mantle wedge structure.

ECr4 is the southwesternmost line in our survey and traverses the Oki-Hateruma Basin at the southern end. The thicknesses of materials with $V_p < 5$ km/s below the arc area of ECr4 are thicker than those of ECr5, and the upper crustal structure for ECr4 is different from that for ECr5. However, the thickness of low-V_p materials for ECr4 is much thinner compared to ECr16 and ECr6. A middle crust with a V_p of 6.1–6.5 km/s and a thickness of about 10 km is underlain by a lower crust with a V_p of 6.8–6.9 km/s and a thickness of about 5 km. A small velocity gap, between 6.2 and 6.3 km/s, in the middle crust is modeled based on the reflection signals observed in several OBSs. The MCS profile (Fig. 3) shows a thick sedimentary layer with the maximum thickness of 3 km and a V_p of less than 3.5 km/s beneath the Oki-Hateruma Basin. Although the image of the subducting PHS plate was not determined in the V_p model, clear reflection signals at a depth of ~20 km under the forearc basin, inferred as reflections from the plate interface, were detected in the MCS profile (Fig. 3).

Island arc (ECr31) and forearc (ECr25)

We shot ECr31 and ECr25 along the island arc and forearc, respectively (Fig. 1). The MCS records and V_p models for these seismic lines are shown in Fig. 7. The checkerboard test results and ray diagrams are presented in Fig. 5.

ECr31, with a length of 228 km, crosses the Miyako Saddle at the southwestern end and the Kerama Gap at the northeastern end. This line crosses ECr7, ECr6, and ECr16 from southwest to northeast, and the shallower parts of their V_p models at the intersections are consistent with each other. The MCS record for ECr31 shows many normal faults beneath the Miyako Saddle and the Kerama Gap. Two distinctive reflectors at depths of 1–2 and 3–4 km were observed beneath the Miyako Saddle, and they are cut by many normal faults. The deeper reflector at a depth of 3–4 km corresponds to the top of the upper crust based on its V_p model (Fig. 7). In contrast, the reflectors beneath the Kerama Gap are significantly discontinuous due to the large offsets of the normal faults indicating larger deformation in this region.

We obtained a horizontally varying arc V_p model that has a middle crust with V_p of 6.1–6.5 km/s and a lower crust with V_p of 6.8–7.0 km/s. Since the velocity gradient in the lower crust is small, we could use only the signals that propagated within the top of the lower crust. Therefore, the V_p of the base of the lower curst and the arc Moho depth of around 30 km were inferred using PmP arrivals. At the southwestern end of the line where the Moho depth could not be constrained, the Moho depth is deeper by 2–3 km than the depths estimated at the intersections with ECr6 and ECr16. Some reflection signals from deeper than the Moho depth were also observed, and they may have reflected at the top of the subducting Philippine Sea plate or at its slab Moho. Travel-time mapping (Fujie et al. 2006) of these signals results in many scattered reflectors at depths of 40–60 km, and it is difficult to determine the depths of deeper reflectors precisely.

ECr25 has a length of 415 km from the trench axis at the southwestern end, through the southeastern extension of the Miyako Saddle, to the Kerama Gap at the northeastern end. This line intersects with ECr7, ECr6, ECr16, and ECr5, and confirms the V_p models estimated from these crossed lines. The MCS profile (Fig. 7) reveals a few normal faults in the depressed shallow sedimentary layer below the Kerama Gap, with some faults reaching to the seafloor, although their numbers and their magnitudes are much smaller than those along ECr31. These features suggest the extensional deformation prevails in the areas from the island arc to the forearc, and is in progress at the present time.

The V_p model largely varies along the line, and an arc lower crust is not found (Fig. 7). The layer of which top $V_p = 4$–5 km/s is much shallower below and to the southwest of the Miyako Saddle. The MCS record shows clear reflection signals from the top of the subducting PHS plate. The depth of the plate interface was estimated to be around 15 km below the forearc region from both the MCS and V_p results. When we assumed the bottom of the arc crust having a V_p of 6.2 km/s and the top of the oceanic crust having a V_p of 3–4 km/s at the plate boundary, we had good agreement of the reflection signal amplitudes between the observed and synthetic seismograms (Fig. 8).

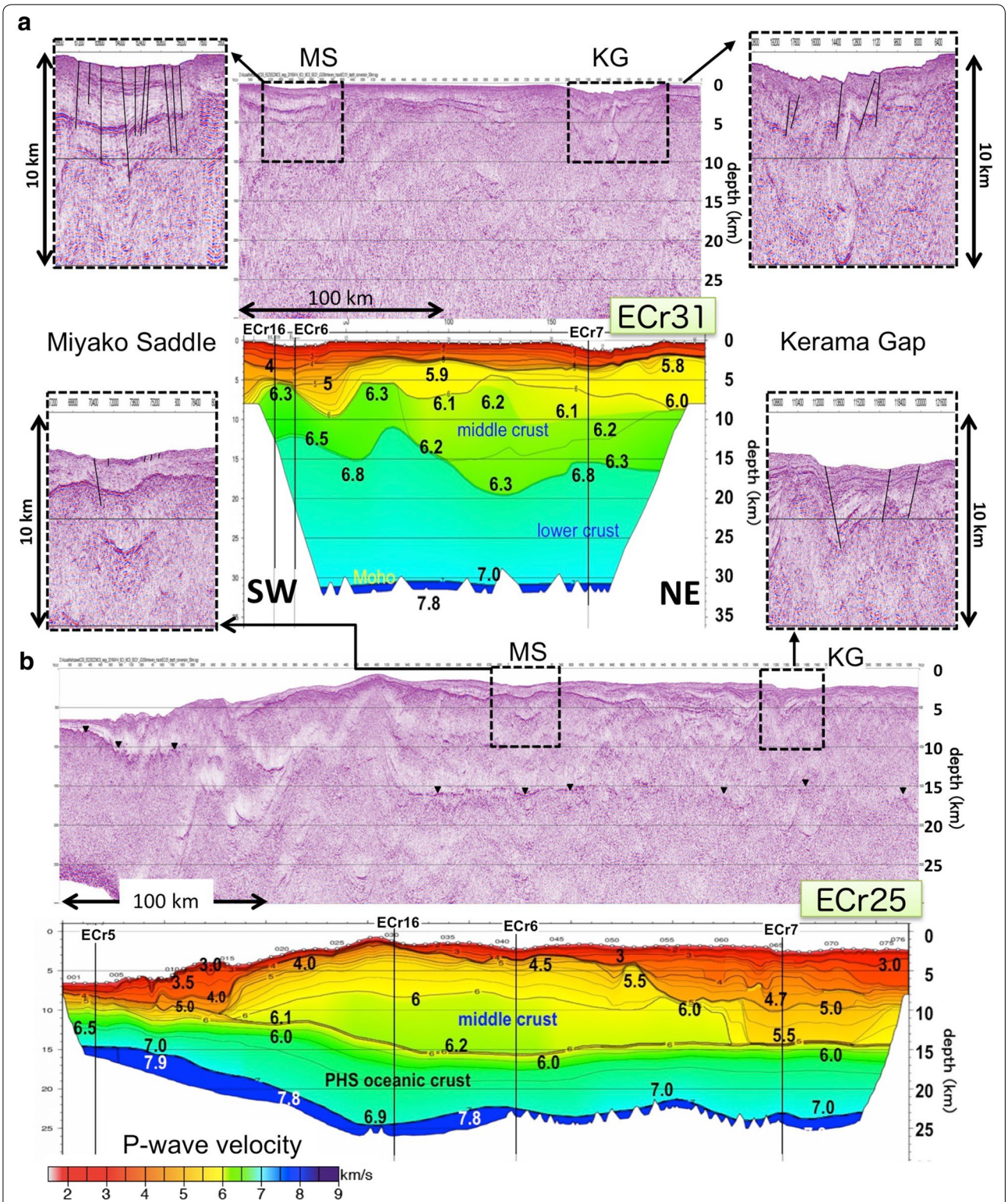

Fig. 7 Depth-converted multichannel seismic section and *P*-wave velocity model for along-forearc lines. **a** ECr31, **b** ECr25. Enlarged seismic reflection images with interpretation for the Kerama Gap and the Miyako Saddle are also shown. The *black lines* in the interpretation indicate steeply dipping normal faults

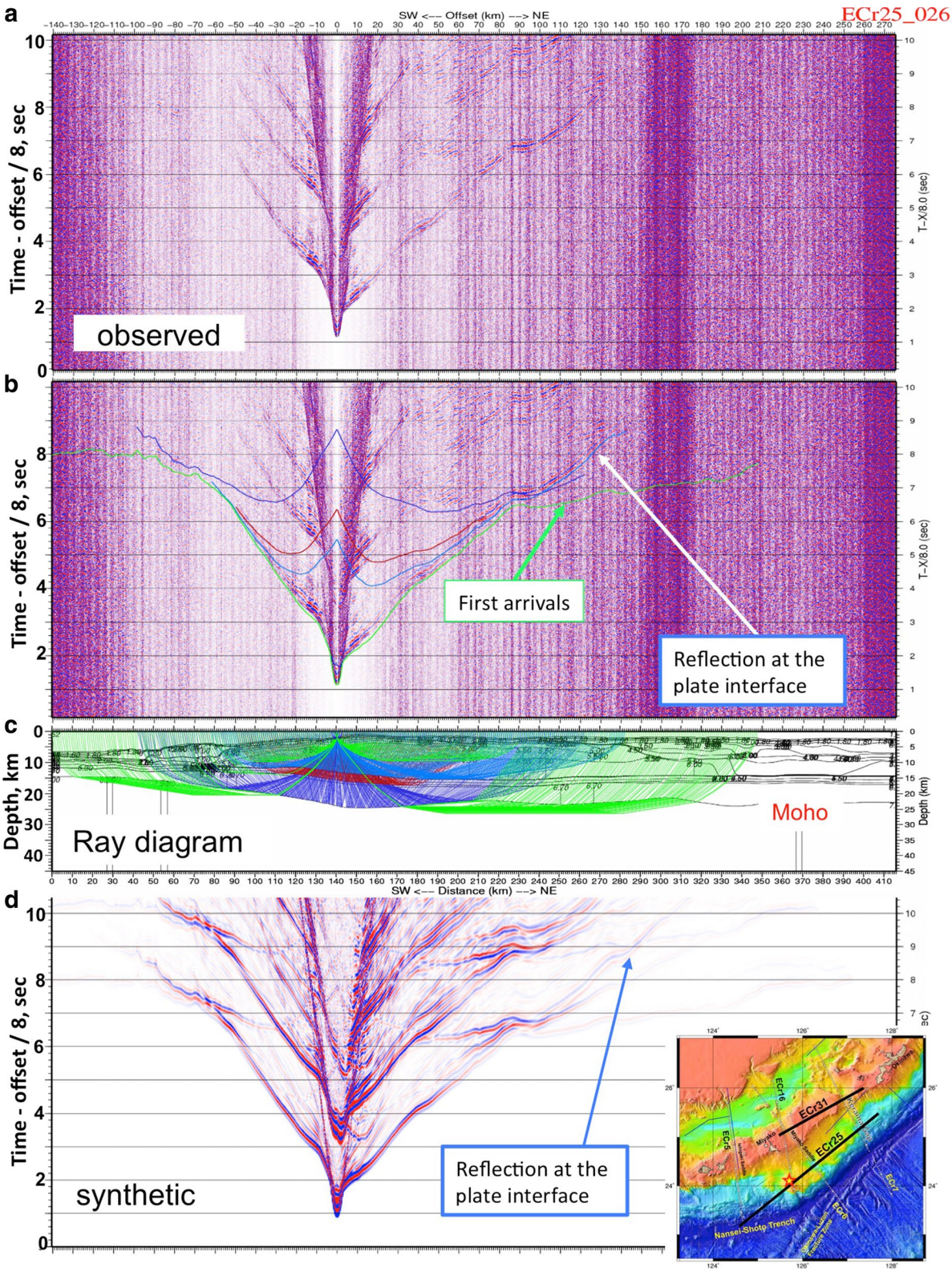

Fig. 8 Observed and synthetic record section for OBS026 on ECr25. **a** Observed vertical record section, **b** observed section with calculated travel times, **c** ray diagram, and **d** synthetic seismogram calculated by E3D code (Larsen and Schultz 1995). The reduction velocity is 8.0 km/s. An *asterisk* in the index map on the *bottom left* shows the position of OBS026

Discussion

Ryukyu island arc

As shown in Fig. 4, the V_p distribution beneath the Ryukyu arc crust varies in the survey lines. However, the arc crust generally consists of three layers: the upper crust (V_p < 6.0 km/s), the middle crust (6.0–6.5 km/s), and the lower crust (6.6–7.0 km/s). Although the V_p of the bottom of each layer could not be well determined, there is a velocity gap between the layers in many cases. The V_p model of ECr31, along the arc line, reveals a typical island structure, the same as the Japan arc compiled by Iwasaki and Sato (2009). A high V_p of around 7.2 km/s at the bottom of the lower crust beneath intra-oceanic island arcs, such as the Izu-Ogasawara island arc and the Kyushu-Palau Ridge (e.g., Nishizawa et al. 2006, 2016), was not found in the Ryukyu arc. None of the arc crusts of the Japan Islands have such a high V_p at the bottom of the lower crust, which might indicate differences in the evolution tectonics between the intra-oceanic island arcs and the Japan island arcs. We deduced a very thin arc lower crust below ECr16 and ECr4 from interpretation of reflected waves at the middle/lower crust boundary and Moho discontinuity, which might relate to the rifting structure of along-arc extension. However, more data are necessary to confirm the deeper part of these models.

Deformations with many normal faults reaching the seafloor at the Kerama Gap and Miyako Saddle are clearly identified in the MCS record of ECr31, which suggests an along-arc extension is ongoing at the present time. The *P*-wave velocities of the upper crust with V_p < 6 km/s and middle crust with V_p of 6.1–6.5 km/s vary along ECr31. Their thicknesses also change along the line. The thickness and V_p of the upper crust beneath the Miyako Saddle are thinner and slower compared with those of the surrounding area. In contrast, the upper crust below the Kerama Gap is thick and the V_p is higher than that below the Miyako Saddle. Therefore, there are no common characteristics in the V_p models between the two bathymetric depressions, and the topographic deformation may not extend to the depth of the upper crust beneath the Kerama Gap.

Ryukyu forearc

There are few significant systematic variations in the forearc seismic structures between the northern and southern Ryukyu Trench except that the low-velocity frontal wedge is much wider in the north and it becomes smaller as it goes to the south. However, there is a characteristic feature of thick, low-velocity wedges with V_p <~4.5 km/s below the forearc regions except for the lines of ECr6 and ECr16. V_p models in the forearc areas for ECr6 and ECr16 reveal that the top of the ~5 km/s layer is much shallower, which is confirmed by the results of ECr25 of an arc-parallel line. The higher free-air gravity anomaly shown in Fig. 2a corresponds to the shallow ~5 km/s materials in this area. The region also corresponds to a lower seismicity compared with other forearc regions, as shown in Fig. 2b. Comparisons of the gravity profiles between ECr11 and ECr6 are shown in Fig. 9. The peak of the high free-air gravity anomaly at the forearc of ECr6 corresponds to high V_p > 5 km/s materials. Although we do not distinguish the origin of the materials from our data, Okamura et al. (2017) interpret that the top of the V_p > 5 km/s layer corresponds to the basement in this region and that the basement does not subside other than the northern and western forearc regions where the basal erosion by subducting bathymetric highs could be enhanced.

There are across-arc normal faults in the MCS records of ECr25 below the Kerama Gap and Miyako Saddle, although they are much smaller in scale than those of ECr31, which indicates the along-arc extension regime continues in the forearc region. The across-arc depressions with a number of normal faults seem to be formed by extension due to backarc extensional rifting of the Okinawa Trough and the trench retreating as suggested by Eguchi (2017). However, recognizable variations in V_p distribution related to these topographic depressions were not observed, similarly to ECr31, indicating that the extensional regime has not influenced the deeper crust.

Another characteristic forearc structure is the influence of specific topographies on the subducting PHS plate. For instance, subduction of the Amami Plateau can be imaged by both the MCS and the V_p model beneath ECr10. Similarly, inhomogeneity due to LOFZ can be detected in the middle part of the Ryukyu Trench.

Subduction of the Philippine Sea plate

The V_p structure of the subducting PHS plate naturally reflects its seafloor topography. The slightly low V_p of 7.6 km/s in the uppermost mantle along the southeastern end of ECr11 is same as the upper mantle velocity beneath the Amami Plateau obtained by Nishizawa et al. (2014). The Pn velocity at northern end of DAr5, to the east of ECr11, is slightly higher V_p of 7.8–8.0 km/s (Nishizawa et al. 2014), which indicates less influence of the Amami Plateau. In the southern seismic lines of the Ryukyu Trench, Pn velocities in the southeastern end of the ECr7 and ECr6 are 7.7–7.9 and 7.8 km/s, respectively, which are slightly smaller than ~8.0 km/s obtained in the Shikoku Basin, the backarc basin on the PHS plate to the east (Nishizawa et al. 2011). These slower Pn velocities in the region might be related to the LOFZ on the PHS plate.

The MCS depth images were more useful in estimating the continuity of the subducting PHS plate interface than

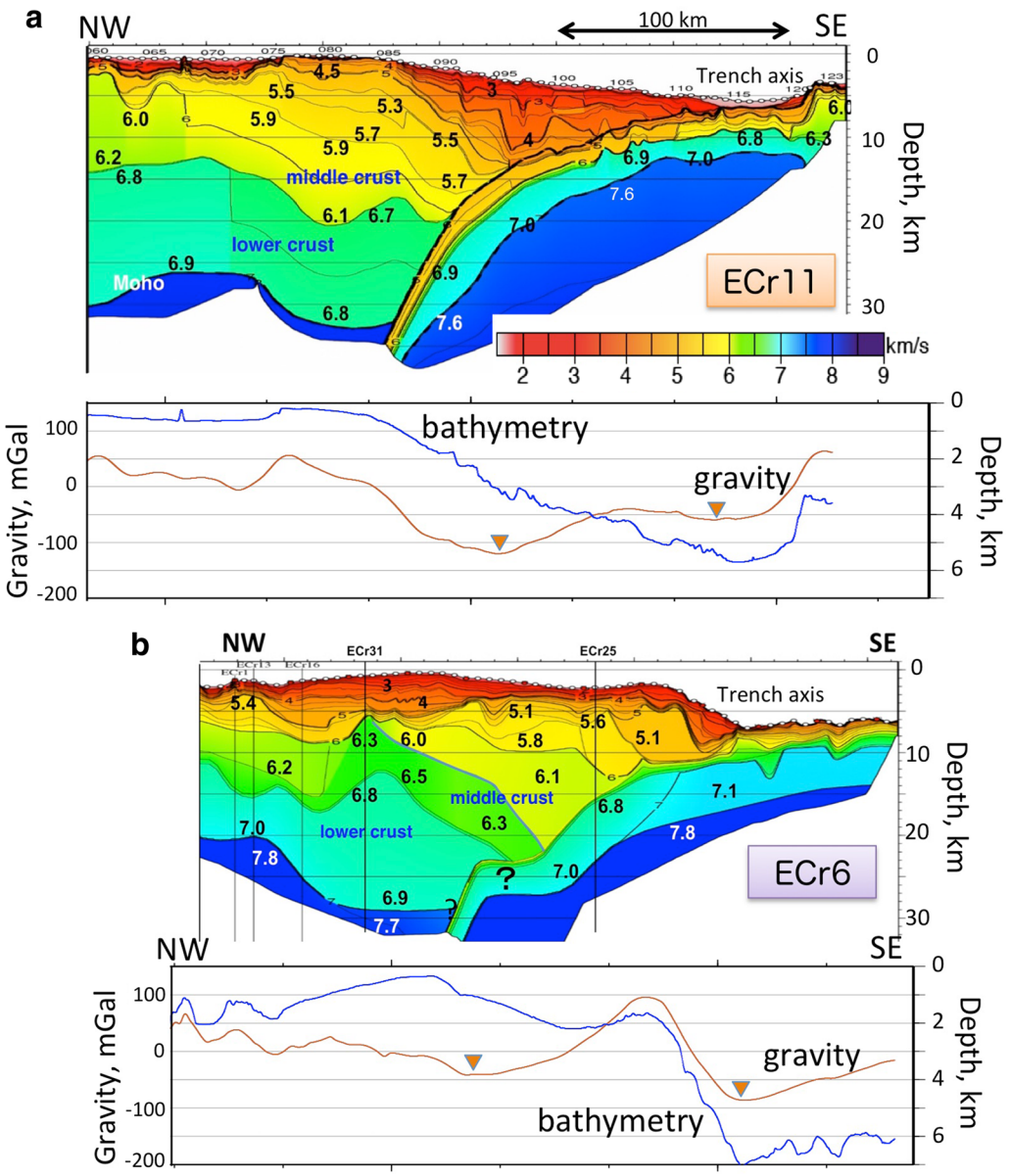

Fig. 9 V_p model and free-air gravity anomaly. Two low gravity peaks are shown by *triangles* on each gravity profile. **a** ECr11 and **b** ECr6

the results of the refraction survey. We compared our estimated interface depths with the iso-depth contours of the plate interface of the Slab 1.0 model by Hayes et al. (2012) in Fig. 10. The 20-km contour almost coincides with our results. However, the depth of 10 km on our seismic lines to the northeast of ECr11 moves toward the trench axis. Previous results for lines KPr1, DAr5, and DAr2 in the northernmost trench area (Nishizawa et al. 2009) also support trenchward positions of the 10-km contour.

Reflections at the subducting plate interface are intermittent in the MCS profile of ECr5 (Fig. 3), and the depth of the interface was not determined in the V_p model in Fig. 4. In contrast, clear slant reflectors can be traced to a depth of ~25 km, as shown by arrows in the MCS record, and these reflection signals have a negative polarity, indicating an abrupt decrease in velocity at the reflector. Arai et al. (2016) observed similar reflection signals in the vicinity of ECr5, and they suggested the reflector is a possible tsunamigenic fault of the 1771 Meiwa Tsunami (Yaeyama Earthquake: M~8). However, there is no significant deformation at the seafloor. Although several more reflectors are detected beneath the forearc basin,

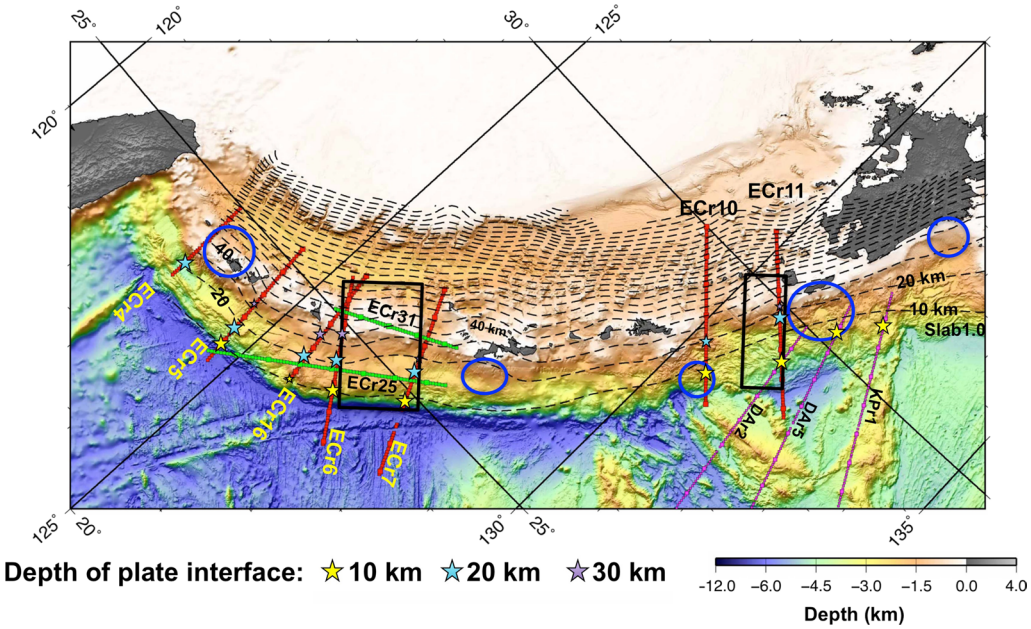

Fig. 10 Depth of the Philippine Sea plate interface (*asterisks*) obtained in this study. *Small asterisks* indicate lower accuracy. *Broken lines* present iso-depth contours of the plate interface with an interval of 10 km (Hayes et al. 2012). *Blue circles* and *black rectangles* show several clusters of short-term slow slip events and the area of poor resolution, respectively (Nishimura 2014)

they do not deform the upper layering structure. Therefore, these faults seem to be inactive lately and they may not be related to the faulting of the 1771 Meiwa Tsunami.

Although the airgun capacity of our MCS survey was only 17.1 L (1050 cubic inches), which is very small for the exploration of deeper structures, we could observe clear reflection signals from the subducting PHS plate interface to maximum depths of more than 25 km. This indicates high pore pressure at the subduction interface in the deeper part and weak interplate coupling in the Ryukyu Trench subduction zone, as Arai et al. (2016) suggested. In contrast, Goto (2013) suggested strong plate coupling caused the 1911 Kikai-jima Earthquake in the northern Ryukyu Trench. The clear reflection signals from the PHS plate interface were not observed deeper than 15 km in the MCS profiles of ECr11 and ECr10, which might correspond to strong coupling at deeper region. Recently, Arai et al. (2017) re-analyzed the ECr10 OBS data together with another MCS profile using a larger airgun array. They interpreted the 1995 Amami-Oshima-Kinkai Earthquake (M7.1) as a near-vertical normal faulting in the subducted part of the Amami Plateau based on the seismic structure and the aftershock distribution inferred from the previous OBS survey (Yamada et al. 1997). Then, they implied the 1911 Earthquake might occur with the similar mechanism of the 1995 event. We need more information about this region to discuss this issue.

Arai et al. (2016) pointed out the relationship between the V_p structure and short-term slow slip events (SSE) estimated by Nishimura (2014). However, we cannot discuss such a relationship through the Ryukyu subduction zone because the positions of our survey lines did not correspond to the SSE source area except for ECr10 (Fig. 10). Nishimura (2014) already pointed out that the SSE area near ECr10 relates to the subduction of the bathymetric high of the Amami Plateau. Seismic lines and seafloor geodetic observations in the area between off Miyako-jima Island and off Okinawa Island are necessary to estimate the interplate coupling in the middle Ryukyu Trench area.

Wells et al. (2003) showed that 70% of coseismic large slip areas of the large earthquakes in the Nankai Trough, northeast of the Ryukyu Trench, occurred beneath forearc basins with a low gravity anomaly. Song and Simons (2003) and Tan et al. (2012) suggested that along-forearc low gravity anomalies parallel to along-trench low gravity zones, that is, double low gravity belts, are related to the occurrence of large earthquakes. This is because the high gravity anomaly area between two low gravity anomaly belts is caused by a large accretionary prism as a result of strong interplate coupling (Tan et al. 2012). Therefore, such gravity anomaly distribution indicates the possibility of large earthquakes in the Ryukyu Trench. Our V_p models of ECr6 and ECr16 in the southern trench show that the distinctive high gravity anomaly between

low gravity belts does not reflect a large accretionary prism but a shallower basement with high V_p velocities (Okamura et al. 2017). This result indicates that strong coupling at the plate boundary is not necessary in this region. Distinct reflection signals from the plate boundary recorded by MCS and OBSs suggest a large velocity gap at the interface beneath ECr25, also indicating a weak interplate coupling.

Muller and Landgrebe (2012) investigated the occurrence of great ($M \geq 8$) subduction earthquakes and found them to be strongly biased toward regions associated with intersections of oceanic fracture zones and subduction zones. How the LOFZ semi-parallel subduction to the trench affects earthquake occurrences is an issue to be addressed in the future.

Conclusions

We shot nine MCS reflection and refraction seismic lines to estimate along-trench variations in the *P*-wave velocity structure of the Ryukyu island arc-trench system. Our results showed the following features:

1. The V_p models below the Ryukyu islands arc crust are heterogeneous, depending on seismic lines, but they generally consist of upper, lower, and middle crusts indicating a typical arc structure.
2. Both the OBS and MCS records revealed the subduction of the Amami Plateau on the PHS plate characterizes the forearc structures below the northern Ryukyu Trench, while there is subduction of the fracture zones beneath the middle and southern trenches.
3. The MCS record showed many normal faults beneath the bathymetric depressions of the Miyako Saddle and Kerama Gap, which indicates an extensional regime along the island arc at present. The V_p models indicate that the deformation below the gaps, however, may not extend to the depth of the middle crust.
4. Several clear reflectors above the subducting plate interface are detected beneath one of the candidate source areas of 1771 Meiwa Tsunami in forearc basin, but they do not deform the upper layering structure. Therefore, these faults seem to be inactive of late and they may not be related to the faulting of the 1771 Meiwa Tsunami.
5. The characteristic high, free-air gravity anomaly at the forearc off Miyako-jima Island is not formed by a large accretionary prism as a result of a strong interplate coupling, but by a shallower basement. The observed clear reflection signals from the plate interface in this area indicate a lower coupling.

Abbreviations

BMFZ: Botan-Miyako fracture zone; CMT: centroid moment tensor; MCS: multichannel seismic; PHS: Philippine Sea; OBS: ocean bottom seismograph; OH: Oki-Hateruma Basin; OLFZ: Okinawa–Luzon fracture zone.

Authors' contributions

AN, KK, MO, DH, YF, and CO contributed to the survey planning, seismic data analysis, and interpretation. AN led interpretation of the seismic records and drafted the manuscript. KK, MO, DH, YF, and CO participated in the seismic surveys and obtained the data. All authors read and approved the final manuscript.

Acknowledgements

The authors gratefully acknowledge Prof. emeritus J. Kasahara, Drs. E. Nishiyama, A. Kamimura, K. Murase, and H. Ohnuma, dedicated technicians of Kawasaki Geological Engineering Co. Ltd., for data processing and analyses. Members of the Continental Shelf Surveys Office, Hydrographic and Oceanographic Department, JCG, are thanked for the management of the seismic surveys. Two anonymous reviewers and the editor, Prof. K Okino, read the manuscript carefully and gave us a lot of constructive comments. Most of the figures in this paper were produced using the GMT graphic package of Wessel and Smith (1998).

Competing interests

The authors declare that they have no competing interests.

Publisher's Note

Received: 6 April 2017 Accepted: 20 June 2017
Published online: 29 June 2017

References

Ando M, Tu Y, Kumagai H, Yamanaka Y, Lin CH (2012) Very low frequency earthquakes along the Ryukyu subduction zone. Geophys Res Lett 39:L04303. doi:10.1029/2011GL050559

Arai R, Takahashi T, Kodaira S, Kaiho Y, Nakanishi A, Fujie G, Nakamura Y, Yamamoto Y, Ishihara Y, Miura S, Kaneda Y (2016) Structure of the tsunamigenic plate boundary and low-frequency earthquakes in the southern Ryukyu Trench. Nat Commun. doi:10.1038/ncomms12255

Arai R, Takahashi T, Kodaira S, Yamada T, Takahashi T, Miura S, Kaneda Y, Nishizawa A, Oikawa M (2017) Subduction of thick oceanic plateau and high-angle normal-fault earthquakes intersecting the slab. Geophys Res Lett. doi:10.1002/2017GL073789

Eguchi T (2017) Arc-parallel extension of forearc region vs. 3-D bending-buckling mode of oceanic lithosphere at subduction zones, JpGU-AGU Joint Meeting 2017, SSS13-01

Fujie G, Kasahara J, Sato T, Mochizuki K (2000) Traveltime and raypath computation: a new method in a heterogeneous medium. J Soc Explor Geophys Jpn 53:1–11

Fujie G, Ito A, Kodaira S, Takahashi N, Kaneda Y (2006) Confirming sharp bending of the Pacific plate in the northern Japan trench subduction zone by applying a traveltime mapping method. Phys Earth Planet Inter 157:72–85. doi:10.1016/j.pepi.2006.03.013

Goto K (2013) Re-evaluation of hypocenter of the 1911 great earthquake around Kikai-jima, Japan. J Seismol Soc Jpn (Zisin) 65:231–242. doi:10.4294/Zisin.65.231

Hayes GP, Wald DJ, Johnson RL (2012) Slab1.0: a three-dimensional model of global subduction zone geometries. J Geophys Res 117:B01302. doi:10.1029/2011JB008524

Hirata N, Kinoshita H, Katao H, Baba H, Kaiho Y, Koresawa S, Ono Y, Hayashi K (1991) Report on DELP 1988 cruises in the Okinawa trough part3. Crustal structure of the southern Okinawa Trough. Bull Earthq Res Inst Univ Tokyo 66:37–70

Hsu SK, Sibuet JC (2005) Earthquake off Japan could generate strong tsunami arrays. EOS Trans AGU 86(17):169–170. doi:10.1029/2005EO170003
Hsu SK, Yeh YC, Sibuet JC, Doo WB, Tsai CH (2013) A mega-splay fault system and tsunami hazard in the southern Ryukyu subduction zone, Earth Planet. Sci Lett 362:99–107. doi:10.1016/j.epsl.2012.11.053
Iwasaki T, Sato H (2009) Crust and upper mantle structure of island arc being elucidated from seismic profiling with controlled sources in Japan. J Seismol Soc Jpn (Zisin) 61:S165–S176 **(in Japanese with English abstract)**
Iwasaki T, Hirata N, Kanazawa T, Melles J, Suyehiro K, Urabe T, Moller L, Makris J, Shimamura H (1990) Crustal and upper mantle structure in the Ryukyu island arc deduced from deep seismic sounding. Geophys J Int 102:631–651
Klingelhoefer F, Berthet T, Lallemand S, Schnurle P, Lee CS, Liu CS, McIntosh K, Theunissen T (2012) P-wave velocity structure of the southern Ryukyu margin east of Taiwan: results from the ACTS wide-angle seismic experiment. Tectonophysics 578:50–62
Kodaira S, Iwasaki T, Urabe T, Kanazawa T, Egloff F, Makris J, Shimamura H (1996) Crustal structure across the middle Ryukyu trench obtained from ocean bottom seismographic data. Tectonophysics 263:39–60
Korenaga J, Holbrook WS, Kent GM, Kelemen PB, Detrick RS, Larsen HC, Hopper JR, Dahl-Jensen T (2000) Crustal structure of the southeast Greenland margin from joint refraction and reflection seismic tomography. J Geophys Res 105:21591–21614. doi:10.1029/2000JB900188
Kubota R, Nishiyama E, Murase K, Kasahara J (2009) Traveltime estimation of first arrivals and later phases using the modified graph method for a crustal structure analysis. Explor Geophys 40:105–113
Larsen SC, Schultz CA (1995) ELAS3D: 2D/3D elastic finite-difference wave propagation code. Lawrence Livermore National Laboratory technical report no. UCRL-MA-121792, pp 19
Lin JY, Sibuet JC, Hsu SK, Wu WN (2014) Could a Sumatra-like megathrust earthquake occur in the south Ryukyu subduction zone? Earth Planets Space 66:49. doi:10.1186/1880-5981-66-49
Matsumoto T, Kimura M, Nakamura A, Aoki M (1996) Detailed bathymetric features of tokara and kerama gaps in the Ryukyu arc. J Geogr 105(3):286–296
Muller RD, Landgrebe TCW (2012) Great earthquakes and oceanic fracture zones. Solid Earth 3:447–465
Nakahigashi K, Shinohara M, Suzuki S, Hino R, Shiobara H, Takenaka H, Nishino M, Sato T, Shinji S, Yoneshim S, Kanazawa T (2004) Seismic structure of the crust and uppermost mantle in the incipient stage of back arc rifting—northernmost Okinawa Trough. Geophys Res Lett 31:L02614. doi:10.1029/2003GL018928,2004
Nishimura T (2014) Short-term slow slip events along the Ryukyu Trench, southwestern Japan, observed by continuous GNSS. Prog Earth Planet Sci 1:22. doi:10.1186/s40645-014-0022-5
Nishizawa A, Kaneda K, Nakanishi A, Takahashi N, Kodaira S (2006) Crustal structure of the ocean–island arc transition at the mid Izu-Ogasawara (Bonin) arc margin. Earth Planets Space 58:e33–e36. doi:10.1186/BF03352594
Nishizawa A, Kaneda K, Oikawa M (2009) Seismic structure of the northern end of the Ryukyu Trench subduction zone, southeast of Kyushu, Japan. Earth Planets Space 61:e37–e40. doi:10.1186/BF03352942
Nishizawa A, Kaneda K, Oikawa M (2011) Backarc basin oceanic crust and uppermost mantle seismic velocity structure of the Shikoku Basin, south of Japan. Earth Planets Space 63:151–155. doi:10.5047/eps.2010.12.003
Nishizawa A, Kaneda K, Katagiri Y, Oikawa M (2014) Wide-angle refraction experiments in the Daito Ridges region at the northwestern end of the Philippine Sea plate. Earth Planets Space 66:25. doi:10.1186/1880-5981-66-25
Nishizawa A, Kaneda K, Katagiri Y, Oikawa M (2016) Crust and uppermost mantle structure of the Kyushu-Palau Ridge, remnant arc on the Philippine Sea plate. Earth Planets Space 68:30. doi:10.1186/s40623-016-0407-3
Okamura N, Nishizawa A, Oikawa M, Horiuchi D (2017) Differential subsidence of forearc wedge of the Ryukyu Arc—records of ancient Philippine Sea Plate motion. submitted to Tectonophysics
Oshida A, Kubota R, Nishiyama E, Ando J, Kasahara J, Nishizawa A, Kaneda K (2008) A new method for determining OBS positions for crustal structure studies, using airgun shots and precise bathymetric data. Explor Geophys 39:15–25
Sella GF, Dixon TH, Mao A (2002) REVEL: a model for recent plate velocities from space geodesy. J Geophys Res. doi:10.1029/2000JB000033
Song TRA, Simons M (2003) Large trench-parallel gravity variations predict seismogenic behavior in subduction zones. Science 301:630–633. doi:10.1126/science.1085557
Tan E, Lavier LL, Van Avendonk HJA, Heuret A (2012) The role of frictional strength on plate coupling at the subduction interface. Geochem Geophys Geosyst 13:Q10006. doi:10.1029/2012GC004214
Wells RE, Blakely RJ, Sugiyama Y, Scholl DW, Dinterman PA (2003) Basin-centered asperities in great subduction zone earthquakes: A link between slip, subsidence, and subduction erosion? J Geophys Res 108(B10):2507. doi:10.1029/2002JB002072
Wessel P, Smith WHF (1998) New, improved version of the Generic Mapping Tools released. EOS Trans AGU 79:579
Yamada T, Hino R, Nishizawa A, Shiobara H, Sato T, Goto K, Kanazawa T, Kasahara J, Shimamura H (1997) Aftershock observation of the 1995 Amami-Oshima-Kinkai Earthquake using ocean bottom seismometers. J Geogr 106:514–524